IEEE Access
Multidisciplinary | Rapid Review | Open Access Journal

Received September 3, 2020, accepted September 24, 2020, date of publication September 28, 2020,
date of current version October 8, 2020.

Digital Object Identifier 10.1109/ACCESS.2020.3027322

Greedy-Gradient Max Cut-Based Fault Diagnosis for Direct Online Induction Motors

SHAFI MD KAWSAR ZAMAN[1], (Member, IEEE),
XIAODONG LIANG[2], (Senior Member, IEEE),
AND LIHONG ZHANG[1], (Member, IEEE)
[1]Department of Electrical and Computer Engineering, Memorial University of Newfoundland, St. John's, NL A1B 3X5, Canada
[2]Department of Electrical and Computer Engineering, University of Saskatchewan, Saskatoon, SK S7N 5A9, Canada

Corresponding author: Xiaodong Liang (xil659@mail.usask.ca)

This work was supported in part by the Natural Science and Engineering Research Council of Canada (NSERC) Discovery Grant RGPIN-2016-04170.

ABSTRACT In this paper, a graph-based semi-supervised learning (GSSL) algorithm, greedy-gradient max cut (GGMC), based fault diagnosis method for direct online induction motors is proposed. Two identical 0.25 HP three-phase squirrel-cage induction motors under healthy, single- and multi-fault conditions were tested in the lab. Three-phase stator currents and three-dimensional vibration signals of the two motors were recorded simultaneously in each test, and used as datasets in this study. Features for machine learning are extracted from experimental stator currents and vibration data by the discrete wavelet transform (DWT). To validate the effectiveness of the proposed GGMC-based fault diagnosis method, its classification accuracy using binary classification and multiclass classification for faults of the two motors are compared with other two GSSL algorithms, local and global consistency (LGC) and Gaussian field and harmonic function (GFHF). In this study, the performance of stator currents and vibration as a monitoring signal is evaluated, it is found that stator currents perform much better than vibration signals for multiclass classification, while they both perform well for binary classification.

INDEX TERMS Fault diagnosis, discrete wavelet transform, induction motors, graph-based semi-supervised learning, greedy-gradient max cut, stator current, vibration.

I. INTRODUCTION

Induction motors are most widely used electric machines in various industrial applications. According to a survey for 0.75 kW to 150 kW induction motors, the following faults regularly occur in induction motors: 7% broken rotor bar faults, 21% stator winding faults, 69% bearing faults, and 3% shaft/coupling and other faults [1]. To improve reliability of critical industrial processes and reduce operational down-time, effective diagnosis for electrical and mechanical faults in induction motors is essential.

Induction motor fault diagnosis methods reported in the literature can be divided into three categories:

1) signature extraction-based approaches, where fault signatures in time and/or frequency domain are extracted from recorded signals, such as voltage, current, vibration and leakage flux, and are employed to diagnose faults. The Motor Current Signature Analysis (MSCA) method is one of the most popular techniques in an industrial environment, and most successful in detecting broken rotor bars or end rings [2], [3]. However, the false fault indication is a common issue using MSCA [3], [4].

2) model-based approaches, which relies on the machine's mathematical modeling under fault conditions [5]–[7]. However, precise motor models are often difficult to develop.

3) knowledge-based approaches, where artificial intelligence techniques are increasingly used for fault diagnosis in complex time-varying and non-linear systems [8]. The knowledge-based approaches are data-driven-based, and do not require creating machine models for faulty conditions. Recent advancement of signal processing and artificial intelligence has attracted renewed interests of induction motors fault diagnosis using machine learning [9]–[11]. Supervised learning [9] is the most commonly used method; semi-supervised learning [10] and deep learning [12] are also reported in the literature in this area.

The associate editor coordinating the review of this manuscript and approving it for publication was Hao Luo.

Machine learning needs datasets recorded from field measurements or lab experiments. Although collecting data in industrial processes is not difficult as condition data are continuously monitored, labeling data samples is a time-consuming and cost-prohibitive task, and requires the expert intervention [13], [14]. Large quantities of labeled samples are required for supervised learning and deep learning. In this regard, semi-supervised learning (SSL) has advantages because only a small amount of labeled data are required to train a classification model from a vast amount of unlabeled data [13], [14].

SSL techniques have been employed to improve efficiency and accuracy of different fault diagnostic systems [14]–[17]. A differential evolution-based positioning optimization algorithm is proposed in [14] to label unlabeled data by a repetitive self-labeling process. Modified kernel semi-supervised locally linear embedding is proposed in [17] for electrical fused magnesia furnace fault diagnosis. SSL has also gained more popularity in the field of induction motors fault diagnosis [10], [12], [16], [18], [19]. The published methods include semi-supervised smooth alpha layering for bearing fault diagnosis [10], semi-supervised label consistent dictionary learning framework for machine fault classification [16], semi-supervised deep learning for induction motor gear fault diagnosis [12], manifold regularization-based semi-supervised learning for bearing fault diagnosis [18], and a deep SSL method for motor planetary gearbox fault diagnosis [19]. All SSL-based induction motors fault diagnosis methods reported in the literature use vibration signals, and mostly deal with an individual fault detection [10], [16], [18].

However, in real life, faults in electric machines might occur in a cascade sequence, a fault at one location in the machine may cause a fault at other location. Therefore, single fault or several different types of faults occurred simultaneously inside the machine are potential scenarios that must be considered for fault diagnosis. The existing SSL methods did not cover this aspect. We will tackle this issue in this paper by considering single- and multi-fault conditions of induction motors through binary classification (an individual fault vs. the healthy case), and multiclass classification (several types of faults and the healthy case).

As one of the main families of transductive semi-supervised techniques, the graph-based semi-supervised learning (GSSL) is among the most popular and most effective semi-supervised learning strategies [14], [20]. GSSL can exploit connectivity patterns between labeled and unlabeled samples to improve classification performance through the nearest neighbor graph, which is built to capture the manifold of the data, the classification is then performed by propagating the information from labeled to unlabeled samples along the edges of the graph [14], [20]. Research using GSSL has been reported in [21]–[25]. GSSL is implemented in the fault detection and classification in PV arrays in [13]. Three GSSL algorithms, local and global consistency (LGC), Gaussian random field (GRF), and graph transduction via alternating minimization (GTAM), are compared using simulated and benchmark datasets in [21]. A greedy-gradient max cut (GGMC)-based bivariate formulation strategy for GSSL is proposed in [22], and the extension of this strategy for multiclass problems is shown in [23], [25]. Multi-label GSSL-based residential load monitoring is proposed in [24].

Although GSSL is considered among the most popular and most effective SSL, to the authors' best knowledge, its application in induction motors fault diagnosis has not been investigated. To fill in this research gap, for the very first time, we propose a GGMC-based direct online induction motors fault diagnosis method in this paper. The datasets used in this study are experimental stator current and vibration signals recorded in the lab for two identical 0.25 HP three-phase squirrel-cage induction motors under healthy, single- and multi-fault conditions. To validate the effectiveness of the proposed method, binary classification and multiclass classification are conducted for faults of the two motors, and the results are compared with other two GSSL algorithms, LGC and Gaussian field and harmonic function (GFHF).

The main contributions of this paper include:

1) propose an effective GGMC-based direct online induction motors fault diagnosis approach using experimental stator current or vibration signals;

2) consider single- and multi-electrical and mechanical faults in the fault profile, and conduct both binary classification and multiclass classification to classify faults of the motors using the proposed approach to evaluate its performance;

3) compare the performance of the proposed GGMC-based approach with other GSSL algorithms, LGC and GFHF; and

4) evaluate the effectiveness of experimental stator currents or vibration as a monitoring signal for the proposed fault diagnosis approach.

The paper is organized as follows: the proposed GGMC-based fault diagnosis method, an overview of the basic principle of GSSL, together with introduction of GGMC, LGC and GFHF algorithms, are provided in Section II; the experimental setup for the two 0.25 HP induction motors connected direct online is explained in Section III; feature extraction using Discrete Wavelet Transform (DWT) and sample features are demonstrated in Section IV; the result analysis is conducted in Section V; and conclusions are drawn in Section VI.

II. THE PROPOSED METHOD AND FUNDAMENTAL THEORY OF GSSL

The proposed GGMC-based fault diagnosis method for direct online induction motors in this paper can be implemented in the following three steps:

Step 1: *Data acquisition through either experiments in a lab or field measurements*. The proposed fault diagnosis approach is based on machine learning, and relies on datasets representing various healthy and faulty machine conditions for the fault classification training purpose. To obtain suitable datasets, in this paper, experiments were conducted in a lab for two three-phase 0.25 HP squirrel-cage direct online

induction motors subjected to healthy, single- and multi-fault conditions under different motor loadings. The three-phase stator currents and three-dimensional vibration signals at the axial (x-axis), vertical (y-axis) and horizontal (z-axis) directions were recorded simultaneously in each test. The monitoring signal selection is essential for fault diagnosis, as not all signals work equally well. In this paper, we choose stator currents and vibration as the monitoring signals and their experimental data serve as the datasets for machine learning. Their effectiveness is evaluated and compared in Section V. The details of the experimental set-up for data acquisition are provided in Section III.

Step 2: *Feature extraction through DWT for the stator current and vibration datasets obtained in Step 1*. The extracted features are later used in machine learning in Step 3. DWT is suitable for computerized implementation of wavelet transform (WT) of an input signal due to the following advantages: 1) the original signal is decomposed into approximation (low-frequency components) and detail (high-frequency components) levels through the multi-resolution analysis (MRA); 2) decomposition levels contain sufficient information of the original signal with significantly less computational time; and 3) scale and shift parameters of WT can be discretized. The DWT of a signal can be represented as follows [26]:

$$DWT\ (j,k) = |s^j|^{-1/2} \sum_k x|k|\psi\left(\frac{t - k\tau s^j}{s^j}\right) \tag{1}$$

where $\psi(t)$ is the wavelet function; $x|k|$ is the input signal; s and τ are the scale and shift parameters, respectively; j and k are positive integers. The details of feature extraction using DWT are discussed in Section IV.

Step 3: *Binary classification and multiclass classification using GGMC to detect faults of induction motors*. Binary classification deals with an individual fault vs. the healthy case; while multiclass classification classifies faults among different single- and multi-faults and the healthy case. They are equally important as similar situations might appear in real life during motor operation. The proposed GGMC-based fault diagnosis approach can be fully evaluated through binary and multiclass classifications. To validate the performance of the proposed approach, other two state-of-the-art GSSL algorithms, LGC and GFHF, are compared with GGMC. The fundamental theory of GGMC, LGC, and GFHF is introduced in this section. The performance of the proposed method is demonstrated in Section V.

The flowchart of the proposed fault diagnosis approach is shown in Fig. 1.

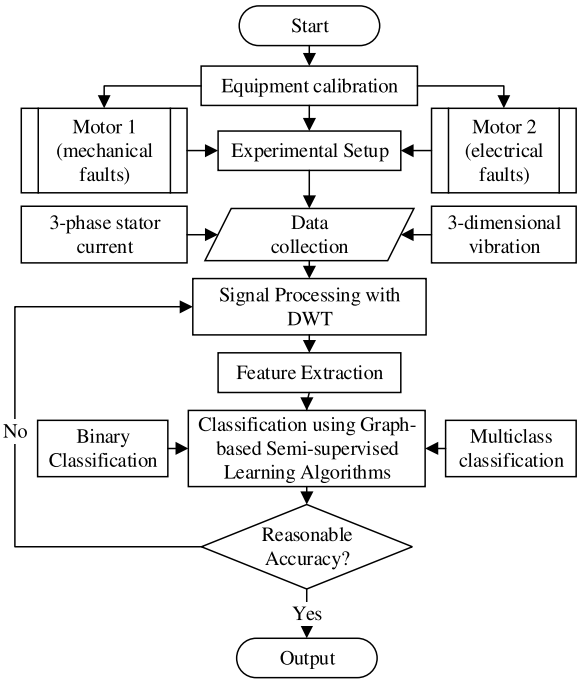

FIGURE 1. The flowchart of the proposed fault diagnosis approach.

A. FUNDAMENTAL THEORY OF GSSL

The GGMC algorithm belongs to the family of GSSL. Before introducing GGMC, we first introduce the basic principle of GSSL. Assuming that a dataset has both labeled and unlabeled data, the GSSL method approximates a weighted sparse graph from the total input data and provide an estimate of unknown labels using known labels. The actual labels are determined later on by optimizing a fitness function chosen appropriately. $G = \{X, E, W\}$ is assumed to be the undirected graph generated from the input data, where the set of vertices is $X = \{x_i\}$ (each sample x_i is a vertex), the set of edges is $E = \{e_{ij}\}$, and the weight matrix is $W = \{w_{ij}\}$. The weight of edge e_{ij} is w_{ij}, the weights for edges are used to construct the weight matrix W. The vertex degree matrix $D = diag([d_1,\ldots, d_n])$ is defined as $d_i = \sum_{j=1}^{n} w_{ij}$. The graph Laplacian is defined as $\Delta = D - W$, and the normalized graph Laplacian can be represented as follows [22]:

$$L = D^{-1/2}\Delta D^{-1/2} = I - D^{-1/2}WD^{-1/2} \tag{2}$$

where Δ is the standard graph Laplacian quantity.

The smoothness measurement of the function space f using L over a graph is defined by [25]:

$$\langle f, Lf\rangle = \sum_i \sum_j w_{ij} \left\| \frac{f(x_i)}{\sqrt{d_i}} - \frac{f(x_j)}{\sqrt{d_j}} \right\|^2 \tag{3}$$

A label matrix is formed as $Y = \{y_{ij}\}$, which contains the label information: $y_{ij} = 1$ if x_i is associated with label j for $j \in \{1,2,\ldots, c\}$(c is the number of classes); otherwise, $y_{ij} = 0$. Let $F = f(X)$ be the classification function over the dataset X. The GSSL algorithms use W and the known labels to minimize a fitness function defined on the graph G and retrieve a continuous classification function F.

The graph can be formulated in two typical ways: 1) the ε-neighborhood graph connecting samples within a distance of ε, and 2) the kNN graph connecting k-nearest neighbors. In practice, a kNN graph is more robust to scale variation and

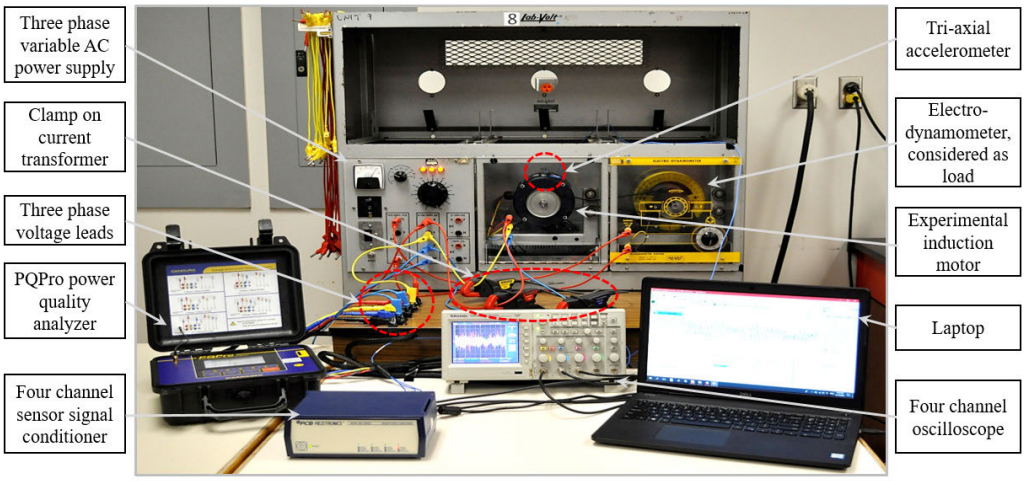

FIGURE 2. Experimental test bench.

abnormalities in the data density [27]. Therefore, the kNN neighborhood graphs are adopted in this paper.

There are two schemes mostly considered for graph edge reweighting: binary edge weighting and fixed Gaussian kernel edge weighting [21]. In this paper, both edge weighting schemes are used in the chosen GSSL algorithms.

B. THREE GSSL ALGORITHMS: GGMC, LGC, AND GFHF

In this paper, three GSSL algorithms are involved: GGMC. LGC and GFHF. GGMC is used in the proposed approach, the effectiveness of the proposed approach is further validated by comparing with LGC and GFHF.

For LGC and GFHF algorithms, a fitness function Q is defined by involving two penalty terms: the global smoothness Q_{smooth} and the local fitting accuracy Q_{fit}. The final classification function F is obtained by minimizing the fitness function Q by [28]

$$\mathrm{F}^{*} = \arg\min_{\mathrm{F}\in\mathrm{R}^{\mathrm{n}\times\mathrm{c}}} \mathrm{Q}\,(\mathrm{F}) = \arg\min_{\mathrm{F}\in\mathrm{R}^{\mathrm{n}\times\mathrm{c}}} \left(\mathrm{Q}_{\mathrm{smooth}}\,(\mathrm{F}) + \mathrm{Q}_{\mathrm{fit}}\,(\mathrm{F})\right) \tag{4}$$

For LGC, the objective function is formulated by [19]

$$Q\,(F) = \|F\|_G^2 + \frac{\mu}{2}\,\|F - Y\|^2 \tag{5}$$

where the first term $\|F\|_G^2$ represents the function smoothness over the graph G, $\|F - Y\|^2$ in the second term estimates empirical losses of the given labeled samples, and the coefficient μ in the second term provides a balance between the global smoothness and the local fitting terms. If $\mu = \infty$ and the standard graph Laplacian quantity Δ for the smoothness term is implemented, Eq. (4) is reduced to GFHF by [29]

$$Q\,(F) = tr(F^T \Delta F) \tag{6}$$

The optimization problem in LGC and GFHF can be broken down into separate problems as additive terms [30]. However, such decomposition method may result in biases if input labels are not balanced proportionally, which may cause inconsistent classification results.

To solve this problem, GGMC was created through a bivariate formulation that explicitly optimizes over both the classification function F and the label matrix Y as follows [14]:

$$Q\,(F, Y) = \frac{1}{2} tr\left(F^T L F + \mu\,(F - Y)^T\,(F - Y)\right) \tag{7}$$

In GGMC, unlabeled vertices are assigned to labeled vertices in a way that lowers the value of the fitness function Q along with the steepest descent direction in the greedy step. To avoid biases, imperfect graph-cuts, the outliers' effect, the weighted connectivity among all unlabeled and labeled vertices are defined to minimize the label imbalance over different classes. In this study, the above formulations are extended to multiclass classification [22], [23], [31].

III. EXPERIMENTAL SETUP

Machine learning datasets used in this paper are obtained through experiments in the lab by testing two direct online induction motors. The experimental set-up is shown in Fig. 2, which contains a direct online induction motor and its load. Each of the two identical three-phase squirrel-cage induction motors used in the testing is rated at 0.25 HP, 4-pole, 208-230/460 V, and 1725 r/min (Model LEESON-101649). Since the two motors are identical in their nameplate ratings, the model and the manufacturer, they are treated as sister units and named "Motor 1" and "Motor 2". A dynamometer was coupled to the motor shaft through a belt pulley, serving as the load of the motor.

An eight-channel power quality analyzer, PQPro by CANDURA Instruments, is used to record three-phase stator currents of the tested motor. A tri-axial accelerometer with a four-channel sensor signal conditioner mounted on top of the motor near the face end is used to record x-, y-, and z-axes vibration signals. The stator currents and vibration signals

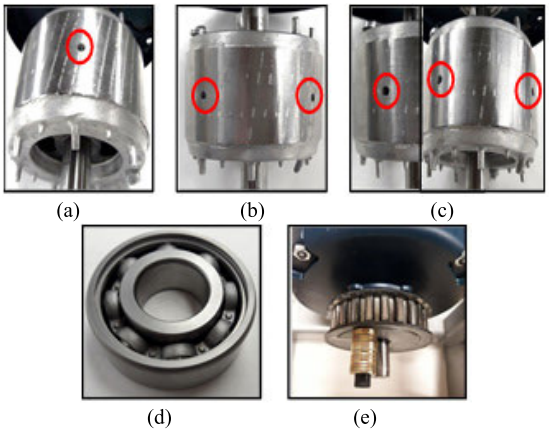

FIGURE 3. Implementation of different faults in the laboratory test bench: (a) One BRB; (b) Two BRBs; (c) Three BRBs; (d) BF; and (e) UNB.

were measured simultaneously for each testing. The sampling frequency for stator currents is 15.38 kHz, and for vibration signals is 1.3 kHz.

The purpose of the testing is data acquisition. Therefore, each induction motor must be tested under healthy and various faulty conditions. To create faulty conditions, the two motors were subjected to different types of single- and multi-faults in the lab.

Motor 1 was mainly used to test different mechanical faults, these faults were created by physically damaging the motor. Five single- and multi-faults were created for Motor 1 and the motor was tested under the following six states: 1) healthy (H); 2) unbalance shaft rotation (UNB); 3) bearing fault (BF); 4) a multi-fault by combining BF and UNB faults (BF+UNB); 5) a multi-fault by combining BF and one broken rotor bar (BRB) faults (BF + 1BRB), and 6) a multi-fault by combining BF, UNB, and unbalanced voltage (UV) condition from the three-phase power supply (BF+UNB+UV).

Motor 2 was mainly used to test different electrical faults, these faults were also created by physically damaging the motor. Five single- and multi-faults were created for Motor 2 and the motor was tested under the following six states: 1) healthy (H); 2) UV from the three-phase power supply (UV); 3) one BRB fault (1BRB); 4) two BRBs fault (2BRB); 5) three BRBs fault (3BRB); and 6) a multi-fault by combining UV and three BRBs faults (UV + 3BRB).

A BRB fault was created by drilling a hole of a 4.2 mm diameter and 18 mm depth in the rotor bar. One hole was drilled for one BRB fault (Fig. 3a); two and three holes with 90° separations were drilled for two and three BRBs faults, respectively (Figs. 3b and 3c). A sandblasting process was used to realize a general roughness type of BF in the motor, and the outer and inner raceway of the bearing became very rough as shown in Fig. 3d. The UNB was created by adding extra weight on the part of the pulley (Fig. 3e). A UV condition was produced by adding extra resistance at the second phase of the motor power supply.

Each motor had 6 states during testing, either healthy or faulty as defined previously. For each motor state, six different motor loadings (10, 30, 50, 70, 85, and 100%) were tested, which leads to 36 testing per motor. A total of 72 tests were conducted for the two motors to cover various healthy or faulty states and motor loading conditions. Only the measured stator currents at the 2nd phase and the vibration at z-axis were used for feature extraction through the DWT.

In this study, the recorded stator current and vibration datasets were selected uniformly with 90,000 data points for each testing of the two motors. The datasets were further partitioned into a fixed window size of 9,000, resulting in 10 data windows for each dataset.

For binary classification, only the healthy and one faulty cases are considered, which lead to 2 class labels for each motor within a data window; since there are 10 data windows for a dataset under each motor loading, it leads to a total of $2 \times 10 = 20$ class labels for a dataset. For multiclass classification, Motors 1 and 2 each has the healthy and five faulty cases, so there are 6 class labels for each motor within a data window; since there are 10 data windows for a dataset under each motor loading, it leads to a total of $6 \times 10 = 60$ class labels for a dataset.

IV. FEATURE EXTRACTION

The DWT in MATLAB's Wavelet Analyzer toolbox is implemented to process the sample data in each data window for feature extraction. Among wavelet families, the Daubechies wavelet with four vanishing moments as db4 is chosen as the mother wavelet with up to the 6th level of decomposition. The following ten time-domain statistical features extracted through DWT for the datasets are selected in this paper: the maximum value of the data window, the minimum value of the data window, mean, median, median absolute deviation, mean absolute deviation, L1 norm, L2 norm, maximum norm, and standard deviation.

Figs. 4 and 5 show the DWT processed vibration and stator current signals for Motor 1 with a BF under 85% and 10% motor loading, respectively, where s denotes the actual signal, a_6 and d_1-d_6 are approximation and detail levels, respectively.

Tables 1 and 2 show samples of features extracted by DWT. Table 1 is for the z-axis vibration signal for Motor 1 with a BF fault under 85% motor loading. Table 2 is for the stator current signal measured at the second phase, I_2, for Motor 1 with a BF fault under 10% motor loading. Every set of ten features in each row of the tables, such as s_1 at the first row of Tables 1 and 2, is processed using DWT by choosing a data window containing 9,000 sample points from the vibration or stator current datasets. Similarly, other nine sets of features (from s_2 to s_{10}) are determined by taking sample points from nine different data windows. The sample of features in each table is extracted based on 10 data windows containing a total of 90,000 sample points as mentioned in previous section.

TABLE 1. The sample of features extracted by DWT using z-axis vibration signal (Motor 1, BF, 85% loading).

Features	Maximum value of data window	Minimum value of data window	Mean	Median	Median Absolute Deviation	Mean Absolute Deviation	L1 norm	L2 norm	Max norm	Standard Deviation
s_1	11.6	-10.6	0.02513	0	0.4	0.626	5605	100.6	11.6	1.06
s_2	11.8	-10.2	0.01864	0	0.4	0.6902	6193	107.1	11.8	1.129
s_3	11	-9.8	0.01622	0	0.4	0.8615	7738	131.3	11	1.384
s_4	9.2	-10.2	0.01804	0	0.4	0.8634	7751	131	10.2	1.381
s_5	11.6	-10.8	0.02324	0	0.4	0.8514	7641	134.3	11.6	1.416
s_6	11	-10	0.02002	0	0.4	0.9179	8244	138.9	11	1.464
s_7	8.6	-8	0.01464	0	0.4	0.7811	7016	120	8.6	1.265
s_8	12.2	-10.8	0.02056	0	0.4	0.8597	7719	137	12.2	1.444
s_9	10.2	-9.6	0.01913	0	0.4	0.9153	8223	139.1	10.2	1.466
s_{10}	9.2	-10.4	0.01847	0	0.4	0.8876	7972	135.5	10.4	1.428

TABLE 2. The sample of features extracted by DWT using stator current I_2 (Motor 1, BF, 10% loading).

Features	Maximum value of data window	Minimum value of data window	Mean	Median	Median Absolute Deviation	Mean Absolute Deviation	L1 norm	L2 norm	Max norm	Standard Deviation
s_1	0.8907	-0.8977	0.004744	0.006474	0.6336	0.5672	5105	59.67	0.8977	0.629
s_2	0.8918	-0.895	0.005388	0.01079	0.635	0.5669	5102	59.63	0.895	0.6286
s_3	0.8923	-0.8923	0.001638	0.001618	0.6301	0.5656	5091	59.58	0.8923	0.6281
s_4	0.8945	-0.8966	-0.001057	-0.00809	0.635	0.5673	5105	59.7	0.8966	0.6293
s_5	0.8891	-0.8907	-0.002501	-0.00728	0.6369	0.5679	5111	59.74	0.8907	0.6297
s_6	0.8961	-0.902	0.0002431	-0.00378	0.6296	0.5658	5092	59.58	0.902	0.6281
s_7	0.8918	-0.8999	0.004226	0.008632	0.6328	0.5665	5098	59.62	0.8999	0.6285
s_8	0.8929	-0.8972	0.005397	0.006744	0.6369	0.5676	5108	59.71	0.8972	0.6294
s_9	0.8961	-0.8902	0.003021	0.005665	0.6299	0.5655	5089	59.51	0.8961	0.6274
s_{10}	0.8955	-0.8999	0.000142	-0.00593	0.6301	0.5651	5086	59.49	0.8999	0.6271

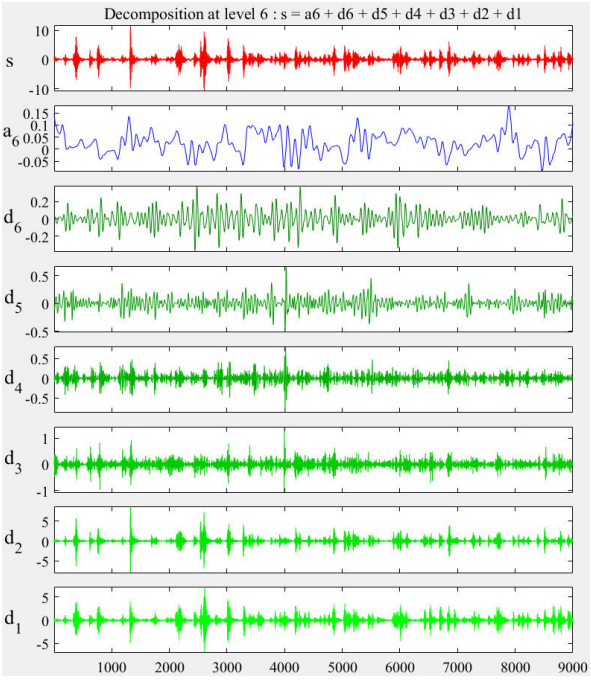

FIGURE 4. The DWT processed vibration signal for Motor 1 (BF and 85% motor loading).

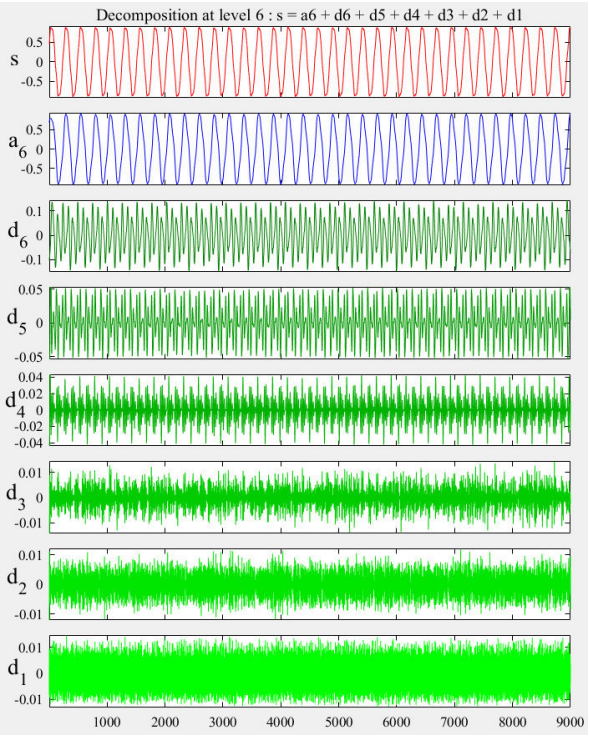

FIGURE 5. The DWT processed stator current signal for Motor 1 (BF and 10% motor loading).

V. RESULT ANALYSIS

In this section, classification accuracy of the proposed GGMC-based fault diagnosis approach is compared with LGC and GFHF through binary and multiclass classification. As previously defined, each of the two motors has six states, either healthy or faulty, which are defined as six classes in machine learning. The set of six classes is

different from Motor 1 to Motor 2: for Motor 1, they are "H", "UNB", "BF", "BF+UNB", "BF + 1BRB", and "BF+UNB+UV"; for Motor 2, they are "H", "UV", "1BRB", "2BRB", "3BRB", and "UV+3BRB".

GGMC, LGC and GFHF are implemented in MATLAB and all run with 100 independent folds with random sampling using the graph construction procedure mentioned in Section II. It is found that GGMC, LGC and GFHF require very similar run-time to output a prediction. For the edge weighting schemes, binary and fixed Gaussian kernel edge weighting are used for the algorithms in the paper. The sparsification is performed using the kNN approach. For the kNN graph construction, $k = 2$ is used uniformly for binary classification for cases between "healthy" and one individual fault; while $k = 4$ is used for multiclass classification for cases with healthy plus five faulty states for each motor. For GGMC and LGC, the value of hyper-parameter $\mu = 0.01$ is used across all cases.

Table 3 shows the parameter settings of the three algorithms, GGMC, LGC and GFHF, used in this work. Table 4 lists the user-defined parameters used to compare the performance of these algorithms.

TABLE 3. Parameter settings of the GSSL algorithms.

GSSL algorithm parameters		Parameter values	
Parameters	GSSL algorithms	Binary classification	Multiclass classification
Number of nearest neighbors, k	LGC, GFHF, GGMC	2	4
Hyper-parameter, μ	LGC, GGMC	0.01	0.01
	GFHF	∞	∞

TABLE 4. User-defined parameters for the GSSL algorithms.

User-defined parameters for executing GSSL algorithms		Parameter values	
Parameters	GSSL algorithms	Binary classification	Multiclass classification
Iteration number	LGC, GFHF, GGMC	100	100
Range of minimum to maximum number of known labels provided	LGC, GFHF, GGMC	2:10	6:30

A. BINARY CLASSIFICATION FOR MOTOR 1

For binary classification for Motor 1, GGMC, LGC and GFHF need a random stratified selection of 2 known labels to ensure at least one representative instance from the two different classes is chosen. The number of known labels gradually increases up to 10 in each case, denoting half of the dataset are labeled. The fault classification performance of GGMC, LGC and GFHF for one individual fault diagnosis of Motor 1 under 50% loading (with 10 known and 10 unknown labels) is shown in Tables 5 and 6 using stator current and vibration, respectively.

In Table 5 using stator currents, the lowest average classification accuracy is 92.5% by LGC and GFHF for a multi-fault (BF+1BRB) vs. healthy case. The highest average classification accuracy is 100% by GFHF and GGMC for the following three faults: a multi-fault (BF+UNB) vs. healthy case, a multi-fault (BF+UNB+UV) vs. healthy case, and a single-fault (UNB) vs. healthy case.

In Table 6 using vibration signal, the lowest average classification accuracy is 96.6% by LGC with the fixed Gaussian kernel edge weighting for a single-fault (UNB) vs. healthy case. The highest average classification accuracy is 100% by GFHF and GGMC for the two faults: a single-fault (BF) vs. healthy case; and a multi-fault (BF+UNB+UV) vs. healthy case.

Tables 5 and 6 indicate that all three GSSL algorithms perform well in general using either stator current or vibration data for individual fault diagnosis, but GGMC consistently perform better than LGC and GFHF.

B. MULTICLASS CLASSIFICATION FOR MOTOR 1

When the multiclass classification is performed for all five faults and the healthy case for Motor 1, there are six different class labels. GGMC, LGC and GFHF were tuned to commence from a random stratified choice of 6 known labels to ensure one representative instance from six classes is chosen. In this case, the number of known labels gradually increases up to 30, denoting half of the dataset are labeled.

Table 7 shows multiclass classification accuracy using stator currents and vibration signals for Motor 1 (with 30 known and 30 unknown labels). From Table 7, using vibration data leads to very low multiclass classification accuracy for all three algorithms, and the highest value is 59% from GGMC with binary edge weighting. However, the classification accuracy is much better using stator currents, and the highest accuracy is 92.53% using GGMC with fixed Gaussian Kernel edge weighting and stator currents.

Fig. 6 shows the multiclass classification accuracy vs. the number of labels using the three GSSL algorithms with binary and fixed Gaussian kernel edge weighting. Both stator currents and vibration data are used for Motor 1 at 50% loading.

From Fig. 6, it is found that the number of labels does not have significant effect on classification accuracies of GGMC, LGC and GFHF, the curves in Fig. 6 appear to be flat throughout a range of number of labels from 6 to 30. This demonstrates the advantage that the chosen graph-based semi-supervised learning algorithms are able to achieve a consistent accuracy using a small amount of labeled data, and this consistency remains true when using both stator current and vibration signals and using both binary and fixed Gaussian kernel edge weighting schemes. GGMC has the highest accuracy compared to LGC and GFHF throughout the range of number of labels from 6 to 30, this proves that our selected method, GGMC, indeed performs better than LGC and GFHF for multiclass classification.

On the other hand, classification accuracies for GGMC, LGC and GFHF using vibration signals shown in dashed

TABLE 5. Binary classification accuracy of GGMC, LGC and GFHF using stator current for motor 1 at 50% loading (with 10 known and 10 unknown labels) (one individual fault vs. healthy case).

GSSL Algorithm	Edge Reweighting Scheme	Average classification accuracy, %				
		H vs. BF	H vs. (BF+1BRB)	H vs. (BF+UNB)	H vs. (BF+UNB+UV)	H vs. UNB
Local and Global Consistency (LGC)	Binary edge weighting	97.3	92.5	99.4	99.4	99.4
	Fixed Gaussian Kernel edge weighting	96.3	92.5	99.7	99.8	99.1
Gaussian Field and Harmonic Function (GFHF)	Binary edge weighting	97.3	92.5	100	100	100
	Fixed Gaussian Kernel edge weighting	97.3	92.5	100	100	100
Greedy- Gradient Max- Cut (GGMC)	Binary edge weighting	97.6	94.5	100	100	100
	Fixed Gaussian Kernel edge weighting	97.3	94.5	100	100	100

TABLE 6. Binary classification accuracy of GGMC, LGC and GFHF using vibration signal for motor 1 at 50% loading (with 10 known and 10 unknown labels) (one individual fault vs. healthy case).

GSSL Algorithm	Edge Reweighting Scheme	Average classification accuracy, %				
		H vs. BF	H vs. (BF+1BRB)	H vs. (BF+UNB)	H vs. (BF+UNB+UV)	H vs. UNB
Local and Global Consistency (LGC)	Binary edge weighting	99.3	97.7	97.8	99.3	97.2
	Fixed Gaussian Kernel edge weighting	98.7	97.1	96.9	98.7	96.6
Gaussian Field and Harmonic Function (GFHF)	Binary edge weighting	100	98.4	97.8	100	97.4
	Fixed Gaussian Kernel edge weighting	100	98.4	97.8	100	97.4
Greedy- Gradient Max- Cut (GGMC)	Binary edge weighting	100	98.4	97.8	100	97.4
	Fixed Gaussian Kernel edge weighting	100	98.4	97.8	100	97.4

TABLE 7. Multiclass classification accuracy of GGMC, LGC and GFHF using stator current and vibration for motor 1 at 50% loading (with 30 known and 30 unknown labels) (five faults and healthy case).

GSSL Algorithm	Edge Reweighting Scheme	Average classification accuracy in % by using vibration	Average classification accuracy in % by using the stator current
Local and Global Consistency (LGC)	Binary edge weighting	55.07	85.27
	Fixed Gaussian Kernel edge weighting	54.3	86.6
Gaussian Field and Harmonic Function (GFHF)	Binary edge weighting	57.63	89.37
	Fixed Gaussian Kernel edge weighting	56.53	89.53
Greedy- Gradient Max- Cut (GGMC)	Binary edge weighting	59	91.83
	Fixed Gaussian Kernel edge weighting	56.6	92.53

TABLE 8. Binary classification accuracy of GGMC, LGC and GFHF using stator current for Motor 2 at 85% loading (with 10 Known and 10 Unknown Labels) (one fault vs. healthy case).

Algorithm		Average classification accuracy, %				
		H vs. 1BRB	H vs. 2BRB	H vs. 3BRB	H vs. (3BRB+UV)	H vs. UV
Local and Global Consistency (LGC)	Binary edge weighting	89.9	100	100	100	98.5
	Fixed Gaussian Kernel edge weighting	89.3	100	100	100	98.5
Gaussian Field and Harmonic Function (GFHF)	Binary edge weighting	94.5	100	100	100	98.5
	Fixed Gaussian Kernel edge weighting	93.6	100	100	100	98.5
Greedy- Gradient Max- Cut (GGMC)	Binary edge weighting	95.1	100	100	100	99.1
	Fixed Gaussian Kernel edge weighting	95.1	100	100	100	98.9

lines in Fig. 6 are much lower than that using the stator current shown in solid lines. Because the accuracies using vibration signals are too low, below 60%, vibration signals are not desirable for multiclass classification for electrical and mechanical faults in induction motors, although they work well for binary classification. From the data acquisition point of view, recording vibration signals from an induction motor requires sensors to be installed on the machine, while the stator currents of the motor can be remotely monitored through the motor control center in a noninvasive way. Therefore, if multiclass classification is desired, the stator current signal is recommended to serve as a monitoring signal.

C. BINARY CLASSIFICATION FOR MOTOR 2

For binary classification of individual fault diagnosis for Motor 2, GGMC, LGC and GFHF were designed to initiate from a random stratified selection of 2 known labels, and the number of known labels was gradually increased up to 10 per dataset. The binary classification performance of GGMC, LGC and GFHF are tabulated in Tables 8 and 9 for Motor 2 at

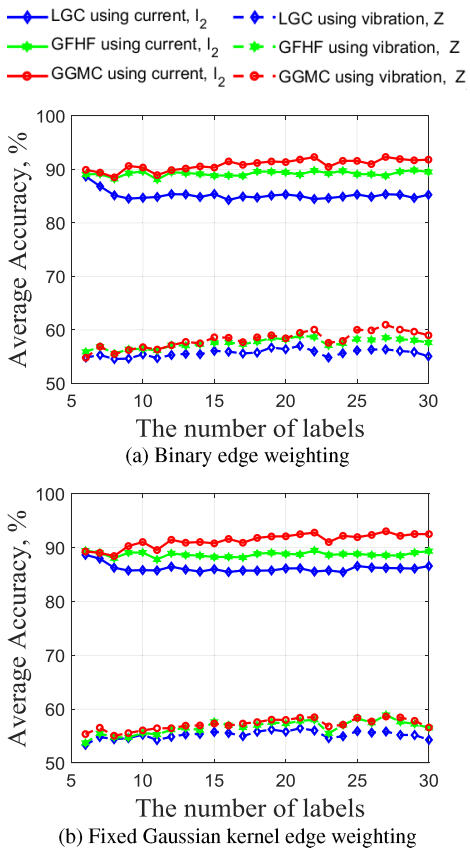

FIGURE 6. Multiclass average classification accuracy vs. the number of labels (for all five faults): Motor 1 at 50% loading.

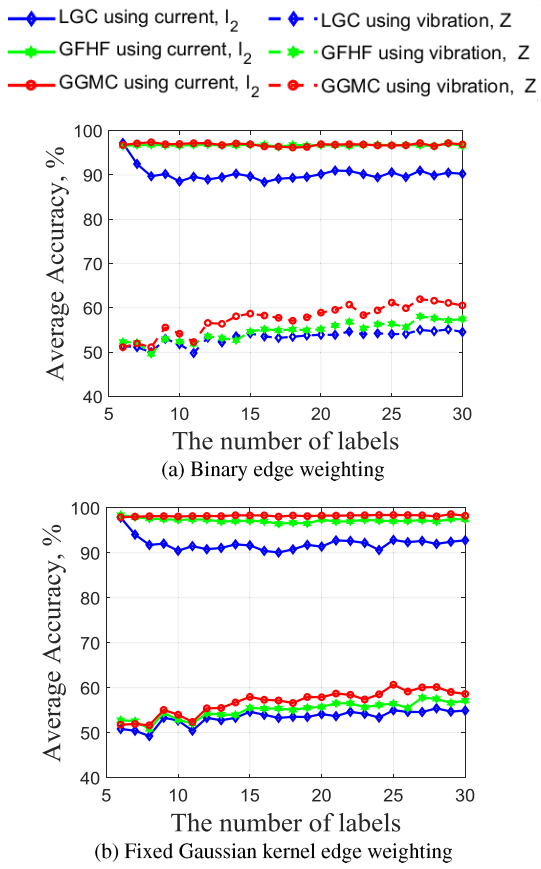

FIGURE 7. Multiclass average classification accuracy vs. the number of labels (for all five faults): Motor 2 at 85% loading.

85% loading (with 10 known and 10 unknown labels) using stator currents and vibration data, respectively.

In Table 8, the lowest average classification accuracy is 89.3% from LGC with the fixed Gaussian Kernel edge weighting for 1BRB vs. healthy case; while the highest average classification accuracy is 100% using GGMC, LGC and GFHF with both edge weighting schemes for the three faults: 2BRB vs. healthy case, 3BRB vs. healthy case, and (3BRB+UV) vs. healthy case.

In Table 9, the lowest average classification accuracy is 61.7% using LGC with the binary edge weighting for 3BRB vs. healthy case; while the highest average classification accuracy is 95.6% using GGMC and GFHF with both edge weighting schemes for the two faults: (3BRB+UV) vs. healthy case, and UV vs. healthy case.

Tables 8 and 9 indicate that all three GSSL algorithms perform well when using stator currents, but they do not perform very well in most cases when using vibration signals. GGMC, however, consistently perform better than LGC and GFHF for all cases.

D. MULTICLASS CLASSIFICATION FOR MOTOR 2

For multiclass classification for Motor 2, there are six different class labels, GGMC, LGC and GFHF were adjusted to start from a random stratified choice of 6 known labels to ensure one representative instance from each class label. The number of known labels to the algorithms was gradually increased up to 30 per dataset.

Table 10 shows multiclass classification accuracy of GGMC, LGC and GFHF for Motor 2 at 85% loading (with 30 known and 30 unknown labels) using stator currents and vibration data. From Table 10, using vibration data leads to very low multiclass classification accuracy for all three algorithms, and the highest accuracy is 60.57% using GGMC with the binary edge weighting. Using stator current leads to much higher multiclass classification accuracy: the lowest accuracy is 90.27% using LGC with the binary edge weighting, and the highest accuracy is 98.27% using GGMC with the fixed Gaussian Kernel edge weighting. GGMC consistently perform better than LGC and GFHF.

Fig. 7 shows multiclass classification accuracy for GGMC, LGC, and GFHF using stator currents and vibration signals vs. the number of labels for Motor 2 at 85% loading.

Similar to multiclass classification for Motor 1 in Fig. 6, from Fig. 7, it is found that the number of labels does not have significant effect on classification accuracies of GGMC, LGC and GFHF for Motor 2, the curves in Fig. 7 are flat throughout a range of number of labels from 6 to 30, showing consistent accuracies for all three algorithms. This further proves through Motor 2 that the chosen graph-based

TABLE 9. Binary classification accuracy of GGMC, LGC and GFHF using vibration for Motor 2 at 85% loading (with 10 Known and 10 Unknown Labels) (one fault vs. healthy case).

Algorithm		Average classification accuracy, %				
		H vs. 1BRB	H vs. 2BRB	H vs. 3BRB	H vs. (3BRB+UV)	H vs. UV
Local and Global Consistency (LGC)	Binary edge weighting	69.4	70.1	61.7	93.8	93.9
	Fixed Gaussian Kernel edge weighting	69.7	83.2	63.7	93.7	95
Gaussian Field and Harmonic Function (GFHF)	Binary edge weighting	82.4	89.9	75.9	95.6	95.6
	Fixed Gaussian Kernel edge weighting	81.7	89.7	75.1	95.6	95.6
Greedy- Gradient Max- Cut (GGMC)	Binary edge weighting	89.3	90.9	85.2	95.6	95.6
	Fixed Gaussian Kernel edge weighting	89.3	89.8	85.2	95.6	95.6

TABLE 10. Multiclass classification accuracy of GGMC, LGC and GFHF using stator current and vibration For Motor 2 at 85% loading (with 30 Known and 30 Unknown labels) (five faults and healthy case).

GSSL Algorithm	Edge Reweighting Scheme	Average classification accuracy in % by using vibration	Average classification accuracy in % by using the stator current
Local and Global Consistency (LGC)	Binary edge weighting	54.93	90.27
	Fixed Gaussian Kernel edge weighting	54.57	92.8
Gaussian Field and Harmonic Function (GFHF)	Binary edge weighting	57.5	96.53
	Fixed Gaussian Kernel edge weighting	57.13	97.43
Greedy- Gradient Max- Cut (GGMC)	Binary edge weighting	60.57	96.9
	Fixed Gaussian Kernel edge weighting	58.63	98.27

TABLE 11. Influence of the number of Features on Binary classification accuracy of GGMC, LGC, and GFHF using stator current for Motor 1 at 50% loading, a multi-fault (BF+UNB+UV) vs. the healthy case (with 10 Known and 10 Unknown Labels).

Algorithm		Average classification accuracy in % for different number of features					
		Case 1	Case 2	Case 3	Case 4	Case 5	Case 6
Local and Global Consistency (LGC)	Binary edge weighting	46	47.3	46.5	49.4	59.9	99.4
	Fixed Gaussian Kernel edge weighting	49.4	49	48.7	57.5	61	99.8
Gaussian Field and Harmonic Function (GFHF)	Binary edge weighting	56.1	56.5	58.3	69.4	91.8	100
	Fixed Gaussian Kernel edge weighting	66.4	67.3	75	86.2	93.5	100
Greedy- Gradient Max- Cut (GGMC)	Binary edge weighting	61.6	70.2	77.9	82.9	93.8	100
	Fixed Gaussian Kernel edge weighting	76.9	79.8	82.6	93.1	94.4	100

semi-supervised learning algorithms are able to achieve a consistent accuracy using a small amount of labeled data. GGMC has similar or slightly better accuracies than GFHF in this case, but significantly better accuracies than LGC. Stator currents show much better performance than vibration as a monitoring signal for multiclass classification for Motor 2.

Based on Tables 5 – 10 for both motors, stator currents perform well for binary classification and multiclass classification, while vibration signals perform well only for binary classification.

E. INFLUENCE OF THE NUMBER OF FEATURES ON CLASSIFICATION

To evaluate the influence of the number of features on binary classification and multiclass classification accuracy using the proposed GGMC-based fault diagnosis method, the following six cases are considered with different number of features:

- Case 1: 4 features (mean, median, L1 norm, and standard deviation).
- Case 2: 5 features (mean, median, mean absolute deviation, L1 norm, and standard deviation).
- Case 3: 6 features (mean, median, median absolute deviation, mean absolute deviation, L1 norm, and standard deviation).
- Case 4: 7 features (mean, median, median absolute deviation, mean absolute deviation, L1 norm, L2 norm, and standard deviation).
- Case 5: 8 features (mean, median, median absolute deviation, mean absolute deviation, L1 norm, L2 norm, maximum norm, and standard deviation).
- Case 6: 10 features (the maximum value of the data window, the minimum value of the data window, mean, median, median absolute deviation, mean absolute deviation, L1 norm, L2 norm, maximum norm, and standard deviation). Case 6 is the chosen method in this study.

GGMC, LGC and GFHF-based binary classification and multiclass classification using stator currents are conducted for the above six cases with different number of features, and their results are compared as shown in Tables 11–14 for the two motors. Tables 11 and 12 are for binary classification: Table 13 is for a multi-fault (BF+UNB+UV) vs. the healthy case for Motor 1 at 50% loading, while Table 14 is for a single-fault (2BRB) vs. the healthy case for Motor 2 at 85% loading. Tables 9 and 10 are for multiclass classification for five faults and the healthy case for Motor 1 at 50% loading and Motor 2 at 85% loading, respectively.

It is found that GGMC shows the best performance compared to LGC and GFHF among all six cases. Case 6 has the highest classification accuracy for all three algorithms

TABLE 12. Influence of the number of Features on Binary classification accuracy of GGMC, LGC, and GFHF using stator current for Motor 2 at 85% loading, a single-fault (2BRB) vs. the healthy case (with 10 Known and 10 Unknown Labels).

Algorithm		Average classification accuracy in % for different number of features					
		Case 1	Case 2	Case 3	Case 4	Case 5	Case 6
Local and Global Consistency (LGC)	Binary edge weighting	47.4	46	49.4	50.3	59.8	100
	Fixed Gaussian Kernel edge weighting	48	48.9	53.3	57.1	60.8	100
Gaussian Field and Harmonic Function (GFHF)	Binary edge weighting	54.8	55.3	58.1	68.7	92	100
	Fixed Gaussian Kernel edge weighting	57.9	60	68.5	80.1	92.2	100
Greedy- Gradient Max- Cut (GGMC)	Binary edge weighting	61.1	70.2	75.5	82.8	93.4	100
	Fixed Gaussian Kernel edge weighting	76	78.4	81.9	90.2	94.1	100

TABLE 13. Influence of the number of Features on Multiclass classification accuracy of GGMC, LGC, and GFHF using stator current for Motor 1 at 50% loading (all five faults and healthy case) (with 30 Known and 30 Unknown Labels).

GSSL Algorithm		Average classification accuracy in % for different number of features					
		Case 1	Case 2	Case 3	Case 4	Case 5	Case 6
Local and Global Consistency (LGC)	Binary edge weighting	29.3	31.9	37.4	66.4	75.8	85.27
	Fixed Gaussian Kernel edge weighting	42.5	51.53	54.8	60.03	81	86.6
Gaussian Field and Harmonic Function (GFHF)	Binary edge weighting	53.4	71.93	77.53	85.5	89.7	89.37
	Fixed Gaussian Kernel edge weighting	69.93	75.83	80.17	84.77	89.4	89.53
Greedy- Gradient Max- Cut (GGMC)	Binary edge weighting	67.27	72.6	79.73	87.97	90.2	91.83
	Fixed Gaussian Kernel edge weighting	71.97	78.33	83.47	86.4	91.73	92.53

TABLE 14. Influence of the number of Features on multiclass classification accuracy of GGMC, LGC, and GFHF using stator current for Motor 2 at 85% loading (all five faults and healthy case) (with 30 Known and 30 Unknown Labels).

GSSL algorithms		Average classification accuracy in % for different number of features					
		Case 1	Case 2	Case 3	Case 4	Case 5	Case 6
Local and Global Consistency (LGC)	Binary edge weighting	38.13	40.6	42.8	49.07	93.1	90.27
	Fixed Gaussian Kernel edge weighting	33.6	38.33	45.17	46.7	93.7	92.8
Gaussian Field and Harmonic Function (GFHF)	Binary edge weighting	60.27	65.7	70.6	86.5	96.4	96.53
	Fixed Gaussian Kernel edge weighting	66.27	69.27	89.6	91.7	96.9	97.43
Greedy- Gradient Max- Cut (GGMC)	Binary edge weighting	70.63	77.23	84.13	90.97	95.93	96.9
	Fixed Gaussian Kernel edge weighting	77.27	77.6	90	91.8	97.77	98.27

compared to Cases 1-5. GGMC has more stable performance when subjected to the variation of the number of features than LGC and GFHF, while LGC performs the worst.

Therefore, it is recommended that the number of features should maintain at either Case 5 or Case 6 to achieve a good classification accuracy for the proposed GGMC-based method.

VI. CONCLUSION

In this study, an effective GGMC-based direct online induction motors fault diagnosis approach is developed. Experimental stator currents and vibration data recorded in the lab for two identical 0.25 HP induction motors under various healthy and faulty states and motor loadings are used as datasets for GGMC. To validate its effectiveness, binary classification and multiclass classification using the proposed GGMC-based approach are conducted and the results are compared with other two GSSL algorithms, LGC and GFHF.

It is found that the proposed GGMC-based approach consistently perform better than LGC and GFHF. Stator currents and vibration data perform well for binary classification, but using vibration data leads to very low multiclass classification accuracy for all three GSSL algorithms, therefore, stator currents are recommended to serve as an effective monitoring signal. GGMC is also more robust than LGC and GFHF when subjected to different number of features. The results of the study demonstrate that an excellent fault classification accuracy can be achieved by the chosen graph-based semi-supervised learning algorithms using a small amount of labeled data.

REFERENCES

[1] A. Bonnett and C. Yung, "Increased efficiency versus increased reliability," *IEEE Ind. Appl. Mag.*, vol. 14, no. 1, pp. 29–36, Jan. 2008.

[2] F. Duan and R. Zivanovic, "Condition monitoring of an induction motor stator windings via global optimization based on the hyperbolic cross points," *IEEE Trans. Ind. Electron.*, vol. 62, no. 3, pp. 1826–1834, Mar. 2015.

[3] S. B. Lee, D. Hyun, T.-J. Kang, C. Yang, S. Shin, H. Kim, S. Park, T.-S. Kong, and H.-D. Kim, "Identification of false rotor fault indications produced by online MCSA for medium-voltage induction machines," *IEEE Trans. Ind. Appl.*, vol. 52, no. 1, pp. 729–739, Jan. 2016.

[4] S. Lee, J. Hong, S. B. Lee, E. J. Wiedenbrug, M. Teska, and H. Kim, "Evaluation of the influence of rotor axial air ducts on condition monitoring of induction motors," *IEEE Trans. Ind. Appl.*, vol. 49, no. 5, pp. 2024–2033, Sep. 2013.

[5] M. Ikeda and T. Hiyama, "Simulation studies of the transients of squirrel-cage induction motors," *IEEE Trans. Energy Convers.*, vol. 22, no. 2, pp. 233–239, Jun. 2007.

[6] M. Sahraoui, A. Ghoggal, S. E. Zouzou, and M. E. Benbouzid, "Dynamic eccentricity in squirrel cage induction motors–simulation and analytical study of its spectral signatures on stator currents," *Simul. Model. Pract. Theory*, vol. 16, no. 9, pp. 1503–1513, Oct. 2008.

[7] A. Berzoy, A. A. S. Mohamed, and O. Mohammed, "Complex-vector model of interturn failure in induction machines for fault detection and identification," *IEEE Trans. Ind. Appl.*, vol. 53, no. 3, pp. 2667–2678, May 2017.

[8] X. Liang and K. Edomwandekhoe, "Condition monitoring techniques for induction motors," in *Proc. IEEE Ind. Appl. Soc. Annu. Meeting*, Oct. 2017, pp. 1–10.
[9] M. Z. Ali, M. N. S. K. Shabbir, S. M. K. Zaman, and X. Liang, "Single- and multi-fault diagnosis using machine learning for variable frequency drive-fed induction motors," *IEEE Trans. Ind. Appl.*, vol. 56, no. 3, pp. 2324–2337, May 2020.
[10] R. Razavi-Far, E. Hallaji, M. Farajzadeh-Zanjani, and M. Saif, "A semi-supervised diagnostic framework based on the surface estimation of faulty distributions," *IEEE Trans. Ind. Informat.*, vol. 15, no. 3, pp. 1277–1286, Mar. 2019.
[11] H. Su and K. T. Chong, "Induction machine condition monitoring using neural network modeling," *IEEE Trans. Ind. Electron.*, vol. 54, no. 1, pp. 241–249, Feb. 2007.
[12] R. Razavi-Far, E. Hallaji, M. Farajzadeh-Zanjani, M. Saif, S. H. Kia, H. Henao, and G.-A. Capolino, "Information fusion and semi-supervised deep learning scheme for diagnosing gear faults in induction machine systems," *IEEE Trans. Ind. Electron.*, vol. 66, no. 8, pp. 6331–6342, Aug. 2019.
[13] Y. Zhao, R. Ball, J. Mosesian, J.-F. de Palma, and B. Lehman, "Graph-based semi-supervised learning for fault detection and classification in solar photovoltaic arrays," *IEEE Trans. Power Electron.*, vol. 30, no. 5, pp. 2848–2858, May 2015.
[14] D. Wu, X. Luo, G. Wang, M. Shang, Y. Yuan, and H. Yan, "A highly accurate framework for self-labeled semisupervised classification in industrial applications," *IEEE Trans. Ind. Informat.*, vol. 14, no. 3, pp. 909–920, Mar. 2018.
[15] M. Grbovic, W. Li, N. A. Subrahmanya, A. K. Usadi, and S. Vucetic, "Cold start approach for data-driven fault detection," *IEEE Trans. Ind. Informat.*, vol. 9, no. 4, pp. 2264–2273, Nov. 2013.
[16] W. Jiang, Z. Zhang, F. Li, L. Zhang, M. Zhao, and X. Jin, "Joint label consistent dictionary learning and adaptive label prediction for semisupervised machine fault classification," *IEEE Trans. Ind. Informat.*, vol. 12, no. 1, pp. 248–256, Feb. 2016.
[17] Y. Zhang, Y. Fu, Z. Wang, and L. Feng, "Fault detection based on modified kernel semi-supervised locally linear embedding," *IEEE Access*, vol. 6, pp. 479–487, 2018.
[18] J. Yuan and X. Liu, "Semi-supervised learning and condition fusion for fault diagnosis," *Mech. Syst. Signal Process.*, vol. 38, no. 2, pp. 615–627, Jul. 2013.
[19] K. Zhang, B. Tang, Y. Qin, and L. Deng, "Fault diagnosis of planetary gearbox using a novel semi-supervised method of multiple association layers networks," *Mech. Syst. Signal Process.*, vol. 131, pp. 243–260, Sep. 2019.
[20] W. Lin, Z. Gao, and B. Li, "Shoestring: Graph-based semi-supervised classification with severely limited labeled data," in *Proc. IEEE/CVF Conf. Comput. Vis. Pattern Recognit. (CVPR)*, Jun. 2020, pp. 4173–4181.
[21] T. Jebara, J. Wang, and S.-F. Chang, "Graph construction andb-matching for semi-supervised learning," in *Proc. 26th Annu. Int. Conf. Mach. Learn. (ICML)*, 2009, pp. 441–448.
[22] J. Wang, T. Jebara, and S.-F. Chang, "Semi-supervised learning using greedy max-cut," *J. Mach. Learn. Res.*, vol. 14, no. 1, pp. 771–800, Mar. 2013.
[23] Z.-J. Zha, T. Mei, J. Wang, Z. Wang, and X.-S. Hua, "Graph-based semi-supervised learning with multiple labels," *J. Vis. Commun. Image Represent.*, vol. 20, no. 2, pp. 97–103, Feb. 2009.
[24] D. Li and S. Dick, "Residential household non-intrusive load monitoring via graph-based multi-label semi-supervised learning," *IEEE Trans. Smart Grid*, vol. 10, no. 4, pp. 4615–4627, Jul. 2019.
[25] S. Wang, X. Guo, Y. Tie, I. Lee, L. Qi, and L. Guan, "Graph-based safe support vector machine for multiple classes," *IEEE Access*, vol. 6, pp. 28097–28107, 2018.
[26] J.-D. Wu and J.-M. Kuo, "An automotive generator fault diagnosis system using discrete wavelet transform and artificial neural network," *Expert Syst. Appl.*, vol. 36, no. 6, pp. 9776–9783, Aug. 2009.
[27] M. Maier, U. V. Luxburg, and M. Hein, "Influence of graph construction on graph-based clustering measures," presented at the Adv. Neural Inf. Process. Syst., 2009, pp. 1025–1032.
[28] Y. Xiu, W. Shen, Z. Wang, S. Liu, and J. Wang, "Multiple graph regularized graph transduction via greedy gradient max-cut," *Inf. Sci.*, vol. 423, pp. 187–199, Jan. 2018.
[29] X. Zhu, Z. Ghahramani, and J. D. Lafferty, "Semi-supervised learning using Gaussian fields and harmonic functions," presented at the 20th Int. Conf. Mach. Learn. (ICML), 2003, pp. 912–919.
[30] J. Wang, S.-F. Chang, X. Zhou, and S. T. C. Wong, "Active microscopic cellular image annotation by superposable graph transduction with imbalanced labels," presented at the IEEE Conf. Comput. Vis. Pattern Recognit., Jun. 2008, pp. 1–8.
[31] W. Liu, J. Wang, and S.-F. Chang, "Robust and scalable graph-based semisupervised learning," *Proc. IEEE*, vol. 100, no. 9, pp. 2624–2638, Sep. 2012.

SHAFI MD KAWSAR ZAMAN (Member, IEEE) was born in Naogaon, Bangladesh. He received the B.Sc. degree in electrical and electronic engineering from the Islamic University of Technology, Gazipur, Bangladesh, in 2014. He is currently pursuing the M.Eng. degree with the Memorial University of Newfoundland, St. John's, NL, Canada.

He was a Visiting Research Student with the Department of Electrical and Computer Engineering, University of Saskatchewan, Saskatoon, SK, Canada, from September 2019 to July 2020. From February 2015 to August 2018, he has served as a Lecturer with the Department of Electrical and Electronic Engineering, Bangladesh University of Business and Technology, Dhaka, Bangladesh. His research interests include conditioning monitoring and fault diagnosis of electric machines using machine learning techniques.

XIAODONG LIANG (Senior Member, IEEE) was born in Lingyuan, Liaoning, China. She received the B.Eng. and M.Eng. degrees from Shenyang Polytechnic University, Shenyang, China, in 1992 and 1995, respectively, the M.Sc. degree from the University of Saskatchewan, Saskatoon, Canada, in 2004, and the Ph.D. degree from the University of Alberta, Edmonton, Canada, in 2013, all in electrical engineering.

From 1995 to 1999, she has served as a Lecturer with Northeastern University, Shenyang, Liaoning, China. In October 2001, she joined Schlumberger in Edmonton, Canada, and was promoted to be a Principal Power Systems Engineer with this world's leading oil field service company in 2009. After serving Schlumberger for almost 12 years, from 2013 to 2019, she was with Washington State University, Vancouver, WA, USA, and Memorial University of Newfoundland, St. John's, Canada, as an Assistant Professor and later Associate Professor. In July 2019, she joined the University of Saskatchewan, where she is currently an Associate Professor. Her research interests include power systems, renewable energy, and electric machines.

Dr. Liang is a registered Professional Engineer in the Province of Saskatchewan, Canada.

LIHONG ZHANG (Member, IEEE) received the Ph.D. degree in electrical engineering from the Otto-von-Guericke University of Magdeburg, Magdeburg, Germany, in 2003. He was a Postdoctoral Research Associate with Concordia University, Montreal, QC, Canada; Dalhousie University, Halifax, NS, Canada; and the University of Washington, Seattle, WA, USA. He is currently a Full Professor with the Department of Electrical and Computer Engineering, Faculty of Engineering and Applied Science, Memorial University of Newfoundland, St. John's, NL, Canada. His current research interests include very large scale integration computer-aided design, mixed-signal integrated system/circuit design, microelectromechanical systems design and optimization, microfluidics and biosensors, wireless sensor networks, and microprocessor-based instrumentation for the ocean and biomedical applications.